PNAS RESEARCH ARTICLE | IMMUNOLOGY AND INFLAMMATION OPEN ACCESS

# Transcription factor EGR2 alleviates autoimmune uveitis via activation of GDF15 to modulate the retinal microglial phenotype

Wanqian Li[a,1], Siyuan He[a,1], Jun Tan[a,1], Na Li[b,1], Chenyang Zhao[a], Xiaotang Wang[a], Zhi Zhang[a], Jiangyi Liu[a], Jiaxing Huang[a], Xingran Li[a], Qian Zhou[a], Ke Hu[a], Peizeng Yang[a], and Shengping Hou[c,2]

Affiliations are included on p. 10.

Edited by Thaddeus Dryja, Harvard Medical School, Boston, MA; received September 17, 2023; accepted July 29, 2024

**Uveitis is a vision-threatening disease primarily driven by a dysregulated immune response, with retinal microglia playing a pivotal role in its progression. Although the transcription factor EGR2 is known to be closely associated with uveitis, including Vogt–Koyanagi–Harada disease and Behcet's disease, and is essential for maintaining the dynamic homeostasis of autoimmunity, its exact role in uveitis remains unclear. In this study, diminished EGR2 expression was observed in both retinal microglia from experimental autoimmune uveitis (EAU) mice and inflammation-induced human microglia cell line (HMC3). We constructed a mice model with conditional knockout of EGR2 in microglia and found that EGR2 deficiency resulted in increased intraocular inflammation. Meanwhile, EGR2 overexpression downregulated the expression of inflammatory cytokines as well as cell migration and proliferation in HMC3 cells. Next, RNA sequencing and ChIP-PCR results indicated that EGR2 directly bound to its downstream target growth differentiation factor 15 (GDF15) and further regulated GDF15 transcription. Furthermore, intravitreal injection of GDF15 recombinant protein was shown to ameliorate EAU progression in vivo. Meanwhile, knockdown of GDF15 reversed the phenotype of EGR2 overexpression–induced microglial inflammation in vitro. In summary, this study highlighted the protective role of the transcription factor EGR2 in AU by modulating the microglial phenotype. GFD15 was identified as a downstream target of EGR2, providing a unique target for uveitis treatment.**

EGR2 | autoimmune uveitis | microglia | GDF15

## Significance

Uveitis is a common vision-threatening disease involving the iris, ciliary body, choroid, retina, and their blood vessels. The results from our previous Genome-wide association analysis (GWAS) study suggest that early growth response 2 (EGR2) genes may modulate the risk of developing Vogt–Koyanagi–Harada disease and Behcet's disease. In this study, we first identified the impact of ERG2 in retinal microglia in a murine experimental autoimmune uveitis (EAU) model. Then, microglia-specific, conditional ERG2 knockout (KO) mice were generated to validate the role of this gene. Next, growth differentiation factor 15 (GDF15) was identified as a target of ERG2 by RNA sequencing (RNA-seq). Finally, intravitreal injection of recombinant GDF15 protein has been shown to alleviate EAU progression in vivo, providing a potential therapeutic strategy for future clinical use.

Uveitis is a vision-threatening disease, affecting the iris, ciliary body, choroid, retina, and associated blood vessels (1). It is categorized into infectious and noninfectious types. The latter, noninfectious uveitis, is mainly linked to immune-mediated factors (2). Autoimmune uveitis (AU) is frequently linked with various systemic diseases, including Vogt–Koyanagi–Harada (VKH) disease, Behcet's disease (BD), and sarcoidosis (3). The exact etiology and pathogenesis underlying AU remain elusive. Current management of uveitis typically involves the administration of corticosteroids and immunosuppressive medications. However, their prolonged use is often hindered by significant side effects or poor tolerance (4, 5). Therefore, there is an urgent need to understand the potential mechanisms and identify therapeutic targets for uveitis to develop more effective and tolerable treatments.

Experimental AU (EAU) targets immunologically privileged retinal antigens and is the most commonly used animal model of AU. It can be elicited using the interphotoreceptor retinol-binding protein (IRBP) (6–8). EAU shares numerous clinical and histopathological features with human AU, serving as a reliable tool for exploring the pathogenesis and therapeutic strategies for uveitis (9–11). Retinal microglia play a critical role in EAU development (12–14). Studies have demonstrated that microglia primarily function to initiate the disease progression, and depletion of microglia prevents immune cell infiltration, thereby halting the progression of the disease progression (15).

Microglia, resident immune cells in the retina, exhibit diverse functions and robust plasticity that are critical for maintaining the dynamic balance of the retinal microenvironment (16). These cells can adopt varying activation phenotypes, mainly classified as proinflammatory and anti-inflammatory states. The proinflammatory state, triggered by lipopolysaccharide (LPS) or interferon gamma (IFN-γ), leads to tissue damage via the secretion of high levels of proinflammatory cytokines and oxidative metabolites. In contrast, the anti-inflammation state induced by IL-4 or IL-10 plays an essential role in suppressing destructive immune responses and repair processes (17). Under normal conditions, microglia continuously monitor the surrounding tissue for damage, pathogens, or abnormal aggregates. Upon detecting these aberrant signals, resting microglia transition into an amoeboid

The authors declare no competing interest.

This article is a PNAS Direct Submission.



[1]W.L., S. He, J.T., and N.L. contributed equally to this work.

[2]To whom correspondence may be addressed. Email: sphou828@163.com.

This article contains supporting information online at https://www.pnas.org/lookup/suppl/doi:10.1073/pnas.2316161121/-/DCSupplemental.

Published September 19, 2024.

morphology. Although activated microglia are able to respond to injury or infection, however, excessive inflammatory responses may exacerbate retinal damage and dysfunction (12, 18). Consequently, understanding the dynamic function of microglia is a major focus in elucidating the pathology of uveitis.

EGR2, a member of the early growth response gene (EGR) family, is a C2H2-type zinc finger transcription factor (19). EGR2 plays a crucial role in myelination and hindbrain development in the central nervous system. In mice, respiratory or feeding disorders caused by EGR2 deficiency lead to perinatal death (20). Increasingly, studies further suggested that EGR2 is involved in the immune response. Notably, EGR2 has been reported to modulate the systemic immune response by suppressing T cells and their cytokine production (21). Additionally, EGR2 has been reported to positively regulate macrophage activation and its plasticity (22, 23). Furthermore, EGR2 exhibits reduced expression in M1 microglia and increased expression in M2 microglia, indicating that it has potential anti-inflammatory effects (24). Significantly, in our previous genome-wide association study in Chinese Han population, a novel locus strongly linked to VKH disease susceptibility, namely the EGR2 locus (rs442309, $P$ combination = $2.97 \times 10^{-11}$, OR = 1.37), was identified (25). This association has also been found in Japanese and Thai populations (26, 27). Moreover, EGR2 has been implicated in BD in Chinese Han and Turkish populations and is expressed in all uveal tissues, including iris, ciliary body, and choroid (28, 29).

Despite evidence suggesting a beneficial role for EGR2 in regulating autoimmune responses, the pathways through which EGR2 exerts its effects in uveitis remain unknown, which constitutes the focus of this study. We reveal that EGR2 expression in microglia is specifically downregulated under inflammatory conditions, both in vivo and in vitro. Conditional knockout of EGR2 aggravated intraocular inflammation in EAU mice, while overexpression of EGR2 reduced the secretion of inflammatory cytokines as well as cell migration and proliferation in human microglia cells (HMC3). Further studies showed that growth differentiation factor 15 (GDF15) was a

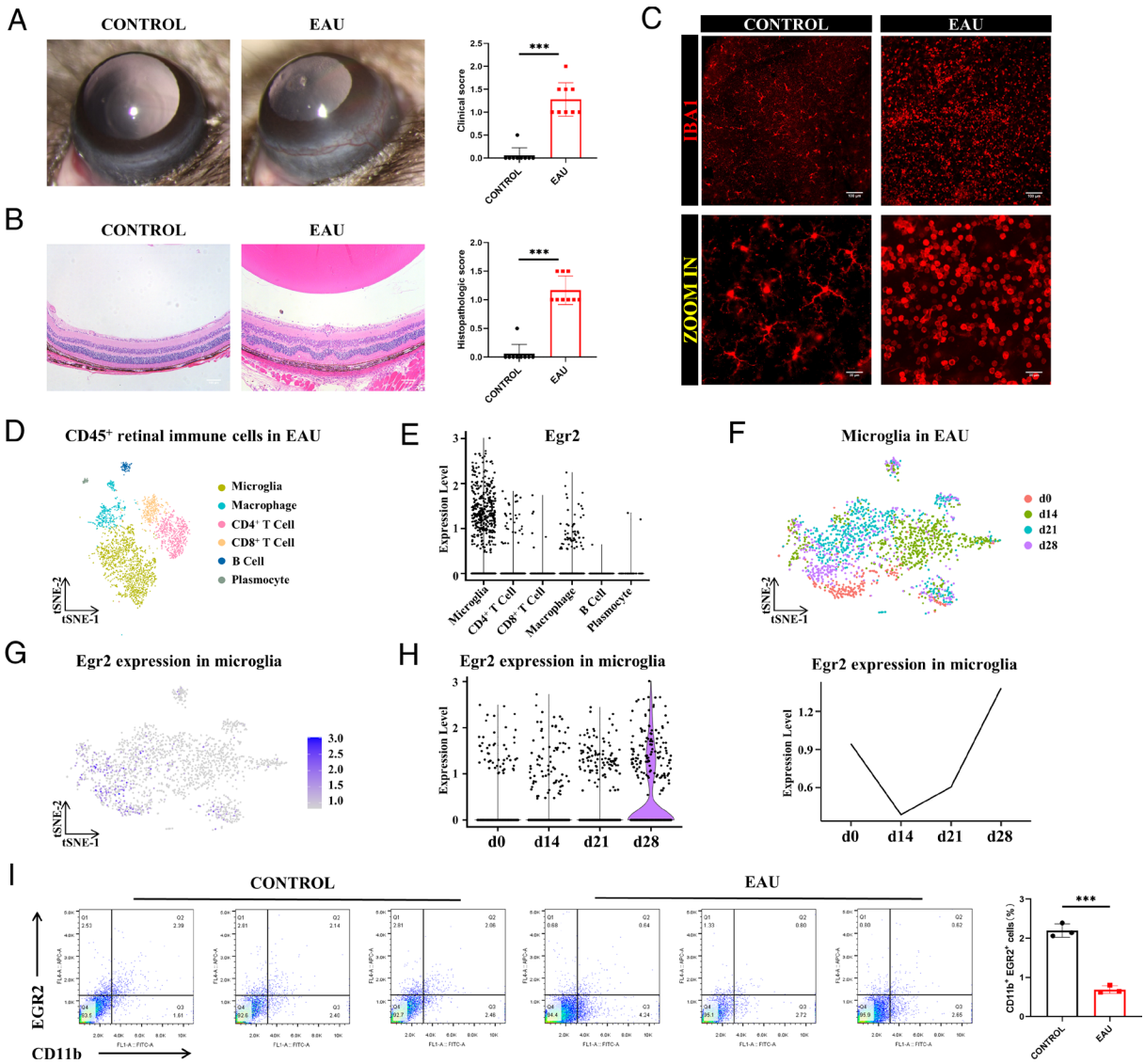


**Fig. 1.** Microglial EGR2 decreased during EAU progression. (*A*) Anterior chamber inflammation in the control and EAU groups. Clinical scores were also shown (n = 9). $^{**}P < 0.01$; Mann–Whitney *U* test. (*B*) Retinal histopathological staining in the control and EAU groups. Pathology scores were also exhibited (n = 9). (Scale bar, 100 μm.) $^{**}P < 0.01$; Mann–Whitney *U* test. (*C*) Retinal flat mount staining with IBA1 (red) in the control and EAU groups (n = 3). Scale bar, 100 μm (*Upper*) and 25 μm (*Lower*). (*D*) t-SNE plot of scRNA-seq exhibited different cell-type clusters in EAU retinas at 0, 14, 21, and 28 d (n = 4). (*E*) The expression level of EGR2 in a total of 4 time points of retinal immune cells of EAU mice (n = 4). (*F*) t-SNE plot of microglia at days 0, 14, 21, and 28 after EAU immunization (n = 4). (*G*) t-SNE plot of EGR2 in microglia at four time points included (n = 4). (*H*) Violin plot and line chart of the expression level of EGR2 at 4 time points in microglia (n = 4). (*I*) Flow cytometric analysis of EGR2 expression in retinal microglia in the control and EAU groups (n = 3). $^{***}P < 0.001$; unpaired Student's *t* test.

downstream target of EGR2, and GDF15 intervention could reverse the protective effect of EGR2 in inflammatory response.

## 1. Results

**1.1. Decreased Expression of Microglial EGR2 during EAU Progression.** First, we constructed a stable EAU mice model which exhibited conjunctival and ciliary hyperaemia, accompanied by inflammation in the anterior chamber (Fig. 1*A*). Retinal histopathological staining showed inflammatory cell infiltration and retinal folds in EAU mice (Fig. 1*B*). In addition, immunofluorescence staining was performed to observe the morphological changes and activation of microglia. The results indicated an increased number of microglia in the retinas of postmodeling mice, characterized by enlarged nuclei, reduced branching, and an activated amoeboid morphology (Fig. 1*C*).

To investigate the underlying mechanisms of EAU, we conducted single-cell RNA sequencing (scRNA-seq) analysis of retinal cells from mice at 0, 14, 21, and 28 d postimmunization, with retinal cells from 4 mice included at each time point. The t-distributed stochastic neighbor embedding (t-SNE) plot, a nonlinear dimensionality reduction algorithm for exploring high-dimensional data, maps multidimensional data into two or more dimensions suitable for observation. Cellular clustering and clustering of single-cell sequencing data by t-SNE plots demonstrated that microglia accounted for the majority of $CD45^+$ retinal immune cells, suggesting that microglia may play a key role in EAU (Fig. 1*D*). Meanwhile, the result indicated that EGR2 was mainly distributed in microglia in retinal immune cells (Fig. 1*E*). To clarify the role of EGR2 in microglia in the pathogenesis of EAU, we depicted the distribution of microglia at 0, 14, 21, and 28 d of EAU modeling. The t-SNE plots demonstrated that microglia were most abundant on day 14 of EAU (Fig. 1*F*). Furthermore, the t-SNE maps demonstrated that EGR2 in microglia at the aforementioned four time points was mainly distributed on day 0 and day 28 after immunization (Fig. 1*G*). The violin plots were generated by analyzing the raw expression of EGR2 in retinal microglia at various stages of EAU, normalized to mitigate differences in sequencing libraries. The mean values calculated by the Average Expression function (the mean value of the data in the expression values of the violin plots converted to exponential form minus 1, and not simply taking the arithmetic mean of the data) were used to plot the EGR2 expression level of the line chart. The results showed that EGR2 expression was lowest at the peak of inflammation on day 14 postimmunization, followed by an increase during the inflammation resolution phases on days 21 and 28 (Fig. 1*H*). In addition, a decreased expression of EGR2 in microglia in the EAU group compared to the control group was verified by flow cytometry analysis (Fig. 1*I*). These findings suggested the involvement of EGR2 in microglia in the development of EAU.

**1.2. Downregulated EGR2 Was Involved in Microglia-Elicited Inflammation In Vitro.** To explore the role and mechanism of EGR2 in microglia, we induced an inflammation model in HMC3 cells using LPS (1 mg/mL) and IFN-γ (500 ng/mL) in vitro. RT-qPCR and western blotting assays revealed increased RNA and protein expression of activation markers of microglia, including iNOS, IL-1β, and TNF-α after 24 h inflammatory stimulation (Fig. 2 *A* and *B*). Subsequently, the wound healing and Transwell assays showed enhanced migration ability of microglia following stimulation (Fig. 2 *C* and *D*). In addition, proliferation of microglia was increased in the LPS+IFN-γ group compared to the control group (Fig. 2*E*).

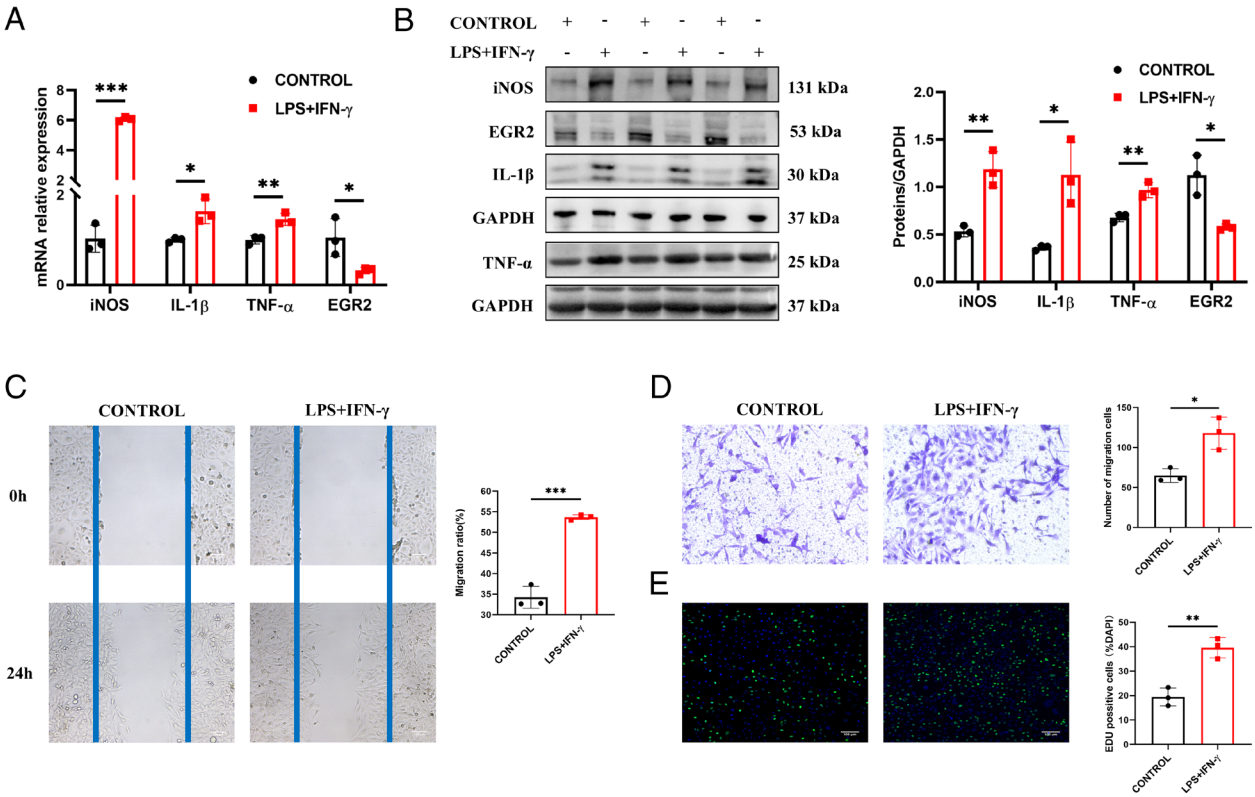


**Fig. 2.** Downregulated EGR2 involved in microglia-elicited inflammation in vitro. (*A*) RT-qPCR to test the relative mRNA expression of iNOS, IL-1β, TNF-α, and EGR2 with or without LPS+IFN-γ treatment for 24 h (n = 3). (*B*) Western blotting assays for the detection of iNOS, IL-1β, TNF-α, and EGR2 in the control and LPS+IFN-γ groups (n = 3). (*C*) Wound healing assay of the control group and LPS+IFN-γ group (n = 3). (Scale bar, 100 μm.) (*D*) Transwell assay to measure cell migration ability in the control and LPS+IFN-γ groups (n = 3). (Scale bar, 100 μm.) (*E*) The EdU assay was used to analyze the proliferation of HMC3 in the control and LPS+IFN-γ groups (n = 3). (Scale bar, 100 μm.) *$P < 0.05$; **$P < 0.01$; ***$P < 0.001$; unpaired Student's *t* test.

Meanwhile, we observed decreased RNA and protein expression levels of EGR2 in HMC3 after inflammatory stimulation, consistent with the in vivo results (Fig. 2 *A* and *B*). Taken together, these findings suggest that downregulation of EGR2 may be strongly associated with the inflammatory response of microglia.

**1.3. EGR2 Conditional Knockout Aggravated EAU Progression In Vivo.** The observation of decreased EGR2 expression following inflammation induction prompted us to construct a CX3CR1-mediated conditional knockout (CKO) mouse model of EGR2 ($CX3CR1^{Cre/Cre}::EGR2^{flox/flox}$) in microglia to further explore the specific role of EGR2 in EAU progression (Fig. 3*A*). The results showed that the clinical and pathological scores of the CKO+EAU group were significantly higher than those of the wild type (WT)+EAU group on day 14 after EAU immunization (Fig. 3 *B* and *C*). Additionally, retinal immunofluorescence staining suggested an increased number of retinal microglia in the CKO+EAU group, displaying a typically activated microglia morphology (Fig. 3*D*). Furthermore, protein expression of iNOS, IL-1β, and TNF-α was markedly elevated in EGR2 knockout mice by the detection of the inflammatory cytokines' secretion in the retina of mice on day 14 (Fig. 3*E*). Therefore, the results suggest that EGR2 deficiency in microglia exacerbates intraocular inflammation in EAU mice.

**1.4. Overexpression of EGR2 Alleviated Inflammation in Microglia In Vitro.** In vitro, we overexpressed EGR2 in HMC3 cells to investigate its regulatory role in microglial function. First, we screened the optimal MOI value for transfection, and the immunofluorescence images showed ideal cell status and transfection efficiency at MOI = 5 (Fig. 4*A*). The efficiency of EGR2 overexpression was evaluated using RT-qPCR and western blotting (Fig. 4 *B* and *C*). Subsequently, HMC3 cells were randomly divided into four groups based on different treatments: the vehicle group, vehicle-LPS+IFN-γ group, oeEGR2 group, and oeEGR2-LPS+IFN-γ group. The results showed increased secretion of inflammatory cytokines after stimulation, while the expression level of the oeEGR2-LPS+IFN-γ group was lower than that of the Vehicle-LPS+IFN-γ group (Fig. 4 *D* and *E*). Both the wound healing assay and Transwell assay confirmed that EGR2 overexpression reduced the migration of HMC3 cells (Fig. 4 *F* and *G*). Additionally, the EDU assay detected reduced proliferation in HMC3 cells following EGR2 overexpression (Fig. 4*H*). These results indicated that increased expression levels of EGR2 could alleviate the inflammatory response in microglia and suggest that EGR2 may act as a regulator of the functional phenotype of microglia.

**1.5. GDF15 Is a Target of EGR2.** To delve deeper into the molecular mechanism by which EGR2 overexpression affects the microglial phenotype, we conducted RNA sequencing (RNA-seq) on the vehicle-LPS+IFN-γ group and the oeEGR2-LPS+IFN-γ group. The volcano plot revealed 412 DEGs with 345 up-regulated and 67 down-regulated (|log2FC| > 1, padj < 0.05) (Fig. 5*A*). Gene ontology (GO) analysis was used to assess the DEGs, revealing the significance of molecular functions related to growth factor binding and receptor–ligand activity (Fig. 5*B*). KEGG analysis showed that EGR2 overexpression was closely associated with

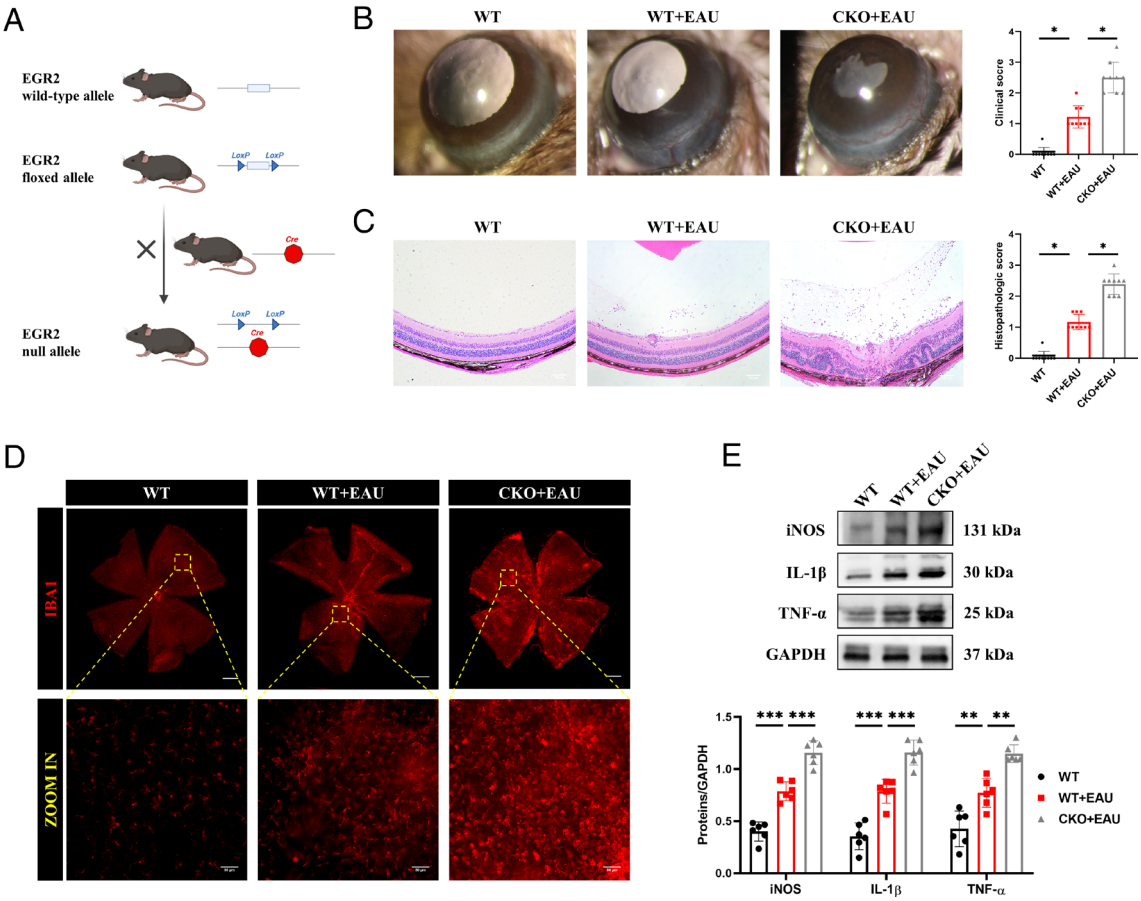


**Fig. 3.** EGR2 knockout aggravated EAU progression in vivo. (*A*) Schematic diagram of the construction of conditional knockout mice. (*B* and *C*) Anterior chamber inflammation and retinal histopathological staining of WT, WT+EAU, and CKO+EAU groups. Clinical scores and pathology scores were also shown (n = 9). (Scale bar, 100 μm.) $^{**}P < 0.01$; Kruskal–Wallias test. (*D*) Retinal microglia fluorescence staining in the WT, WT+EAU, and CKO+EAU groups (n = 3). Scale bar, 500 μm (*Upper*) and 50 μm (*Lower*). (*E*) Protein expression of iNOS, IL-1β, and TNF-α in retina was measured using western blotting (n = 6). $^{*}P < 0.05$; one-way ANOVA.

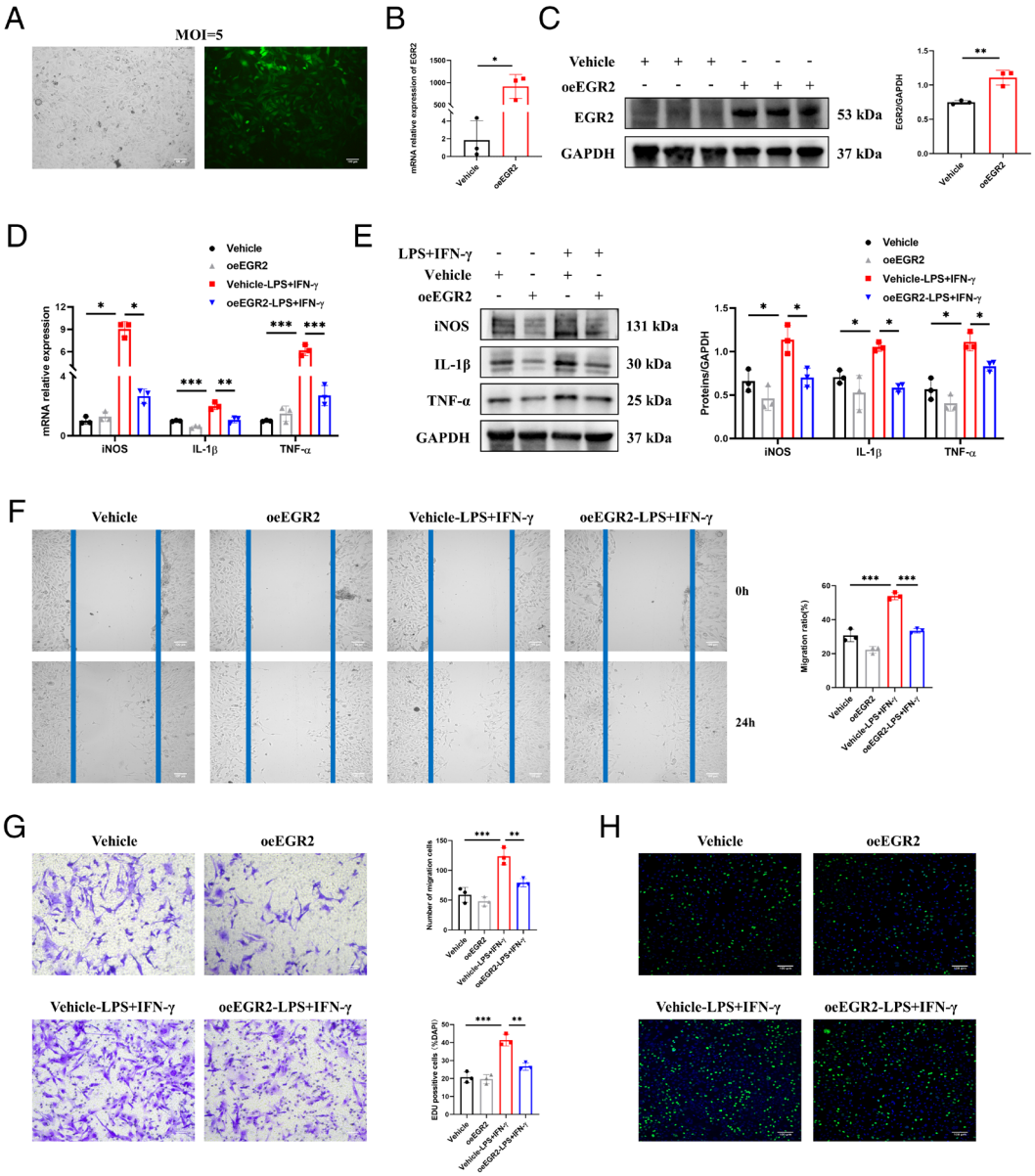


**Fig. 4.** Overexpression of EGR2 alleviated inflammation in microglia in vitro. (*A*) EGFP expression in HMC3 cells transfected with lentivirus. (Scale bar, 100 μm.) (*B* and *C*) Transfection efficiency was assessed by RT-qPCR and western blotting (n = 3). *$P < 0.05$; **$P < 0.01$; unpaired Student's *t* test. (*D* and *E*) RT–qPCR and western blotting assays revealed the expression of iNOS, IL-1β, and TNF-α in the Vehicle, oeEGR2, Vehicle-LPS+IFN-γ, and oeEGR2-LPS+IFN-γ groups (n = 3). *$P < 0.05$; **$P < 0.01$; ***$P < 0.001$; one-way ANOVA. (*F* and *G*) Transwell images, wound healing images, and corresponding quantifications of the vehicle, oeEGR2, vehicle-LPS+IFN-γ, and oeEGR2-LPS+IFN-γ groups (n = 3). (Scale bar, 100 μm.) **$P < 0.01$; ***$P < 0.001$; one-way ANOVA. (*H*) EdU assay to analyze the cell proliferation ability in the abovementioned groups (n = 3). (Scale bar, 100 μm.) **$P < 0.01$; ***$P < 0.001$; one-way ANOVA.

the cytokine–cytokine receptor interaction pathway (Fig. 5*C*). In addition, the heatmap depicted cluster analysis among the 50 most significant DEGs (Fig. 5*D*). Upregulation of the EGR2 gene appeared to mitigate microglial inflammation, possibly due to increased expression of anti-inflammatory genes. Moreover, as a transcription factor, EGR2 can enhance gene transcription by binding to specific DNA sequences in the promoter region. Based on this, five candidate genes were screened and validated by RT-qPCR, among which the GDF15 gene exhibited the most significant increase in expression (Fig. 5*E*). Accordingly, we assessed the protein level of GDF15, which was similarly elevated after EGR2 overexpression (Fig. 5*F*). To ascertain whether GDF15 is a target gene of the transcription factor EGR2, we initially searched the Cistrome Data database, revealing a potential direct binding of EGR2 to the GDF15 promoter (Fig. 5*G*). Next, based on the specific sequence structures of EGR2 and GDF15, the JASPAR website predicted 3 potential sites where the two might bind (Fig. 5*H*). ChIP-PCR assay verified that EGR2 was able to bind to the −1,312 bp to −1,302 bp and −1,670 bp to −1,660 bp regions upstream of the GDF15 transcription start site (Fig. 5*I*). The above results proved that GDF15 is a downstream target of EGR2, and EGR2 could directly regulate the transcription of GDF15. Additionally, we examined the mRNA expression of GDF15 from peripheral blood mononuclear cells (PBMCs) between VKH patients and healthy individuals. However, no significant difference was found in terms of GDF15 expression (*SI Appendix*, Fig. S1).

### 1.6. GDF15 Knockdown Reversed the Effects of EGR2 in Microglia.

To demonstrate the involvement of GDF15 as a downstream of EGR2 in regulating the inflammatory response in microglia, GDF15 was knocked down on HMC3. First, we screened to determine transfection at MOI = 30 (Fig. 6*A*). Next, shGDF15-3, which had

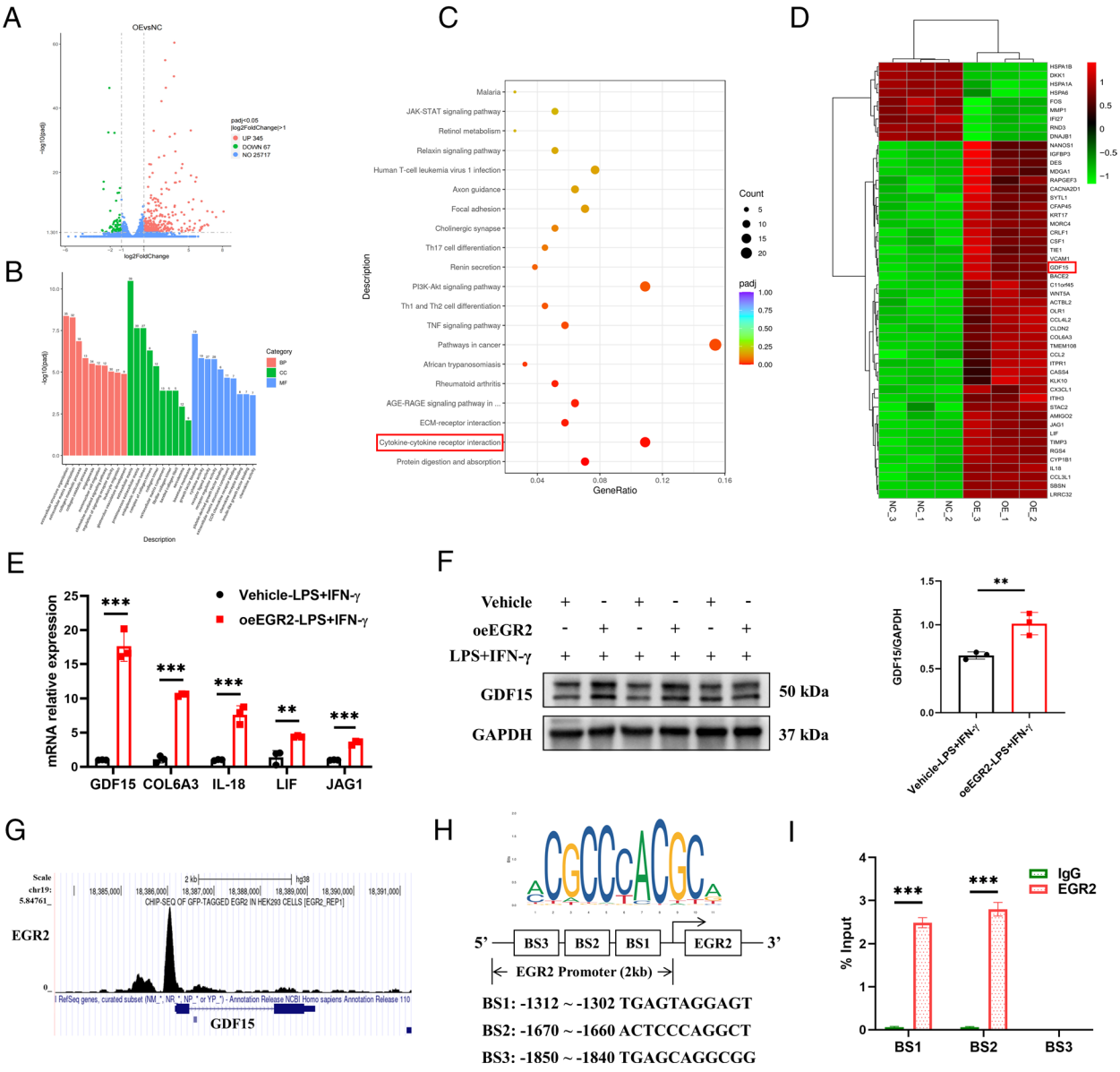


**Fig. 5.** GDF15 is a target of EGR2. (*A*) Volcano plot of DEGs in vehicle-LPS+IFN-γ and oeEGR2-LPS+IFN-γ cells. (*B*) GO analysis of Vehicle-LPS+IFN-γ and oeEGR2-LPS+IFN-γ groups. (*C*) KEGG pathway enrichment analysis in the Vehicle-LPS+IFN-γ and oeEGR2-LPS+IFN-γ groups. (*D*) Heatmap of significant DEGs following EGR2 overexpression. (*E*) The RNA-seq results were verified by RT-qPCR (n = 3). $^{**}P < 0.01$; $^{***}P < 0.001$; unpaired Student's *t* test. (*F*) Western blotting to confirm the protein expression level of GDF15 in the Vehicle-LPS+IFN-γ and oeEGR2-LPS+IFN-γ groups (n = 3). $^{**}P < 0.01$; unpaired Student's *t* test. (*G*) Genomic tracks for ChIP-seq around GDF15. (*H*) Potential EGR2 binding sites of GDF15 promoter. (*I*) ChIP-PCR to validate primers spanning predicted GDF15 promoter sequences (n = 3). $^{***}P < 0.001$; unpaired Student's *t* test.

the most significant knockdown efficiency, was selected for subsequent experiments based on RT-qPCR and WB analysis (Fig. 6 *B* and *C*). The results showed that up-regulated expression of inflammatory cytokines, including iNOS, IL-1β, and TNF-α, in HMC3 after the reduction of GDF15 expression (Fig. 6 *D* and *E*). Meanwhile, both the wound healing and the Transwell assays confirmed that the knockdown of GDF15 markedly recovered the migration ability of HMC3 after inflammatory stimulation (Fig. 6 *F* and *G*). Furthermore, the proliferation of microglia was also enhanced after the reduction of GDF15 expression (Fig. 6*H*). These findings collectively indicated that intervention with GDF15 expression reversed the anti-inflammatory effect of EGR2 overexpression in microglia.

**1.7. Recombinant GDF15 Alleviated EAU Progression In Vivo.** In vivo study, we applied the GDF15 recombinant protein to validate its role as a target of EGR2 in EAU inflammation. The expression of GDF15 was increased by intravitreal injection of recombinant GDF15 (rbGDF15) in mice. As shown in Fig. 7*A*, mice were divided into three groups according to different treatments: WT+EAU group, CKO+EAU group, and CKO+EAU+rbGDF15 group. The clinical and pathological scores of EAU were significantly reduced after rbGDF15 treatment (Fig. 7 *B* and *C*). The results of immunofluorescence also suggested that the addition of GDF15 protein alleviated the microglia phenotype (Fig. 7*D*). In addition, upregulation of GDF15 expression reduced the protein levels of retinal inflammatory cytokines (Fig. 7*E*). The above results suggest that the proinflammatory effect caused by EGR2 knockdown could be reversed by the target GDF15.

## 2. Discussion

In this study, we observed a substantial reduction in the expression of the transcription factor EGR2 within retinal microglia during the inflammatory state. This phenomenon was observed both

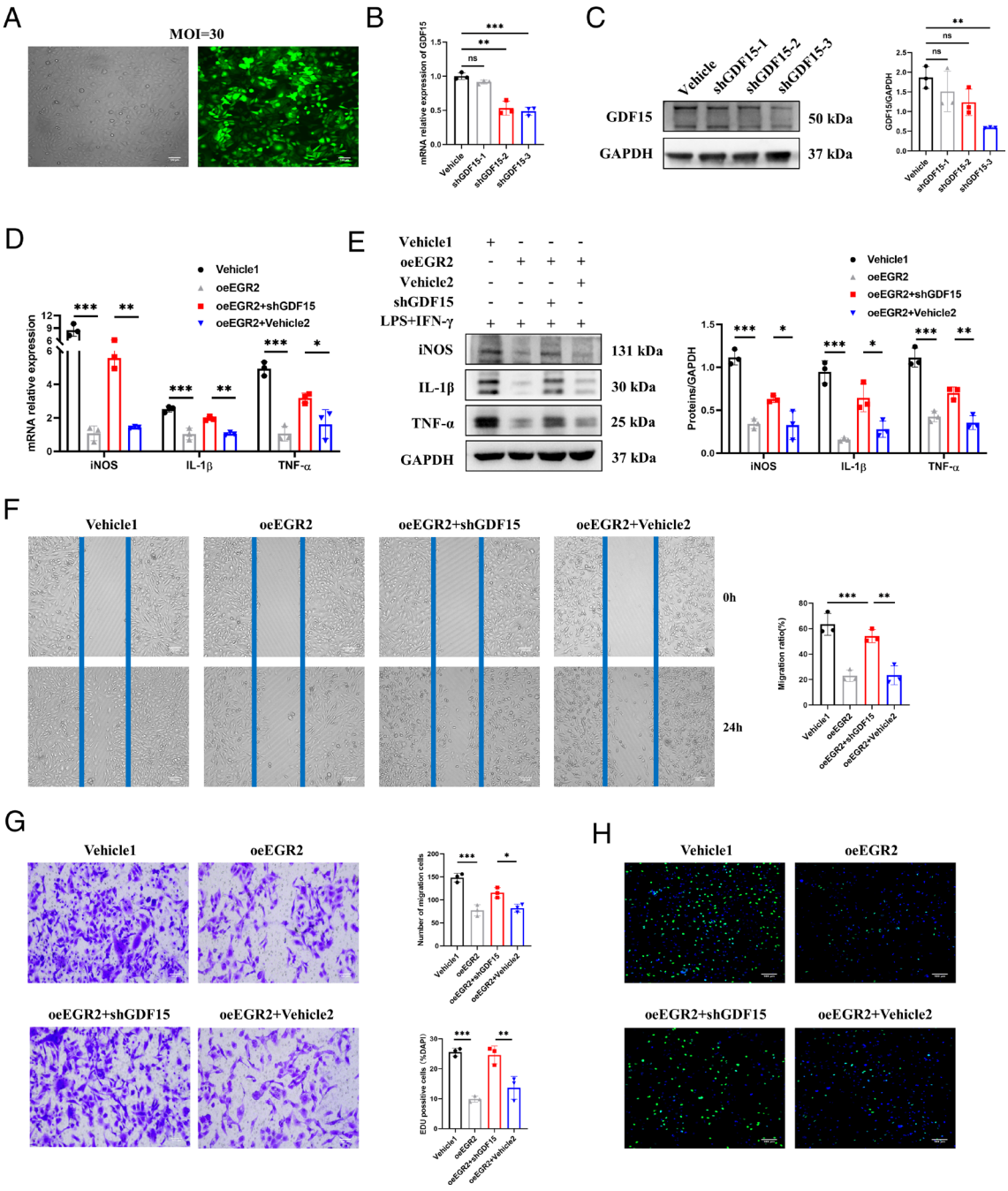


**Fig. 6.** GDF15 knockdown reversed the effects of EGR2 in microglia. (*A*) EGFP expression in HMC3 cells transfected with lentivirus. (Scale bar, 100 μm.) (*B* and *C*) Knockdown efficiency of GDF15 was assessed by RT-qPCR and western blotting (n = 3). ns, $P > 0.05$; $^{**}P < 0.01$; $^{***}P < 0.001$; unpaired Student's *t* test. (*D* and *E*) RT–qPCR and western blotting assays for the detection of iNOS, IL-1β, and TNF-α expression in the Vehicle1, oeEGR2, oeEGR2+shGDF15, and oeEGR2+Vehicle2 groups (n = 3). $^{*}P < 0.05$; $^{**}P < 0.01$; $^{***}P < 0.001$; one-way ANOVA. (*F* and *G*) Transwell images and wound healing images of the abovementioned groups (n = 3). (Scale bar, 100 μm.) $^{*}P < 0.05$; $^{**}P < 0.01$; $^{***}P < 0.001$; one-way ANOVA. (*H*) EdU assay of the Vehicle1, oeEGR2, oeEGR2+shGDF15, and oeEGR2+Vehicle2 groups (n = 3). (Scale bar, 100 μm.) $^{**}P < 0.01$; $^{***}P < 0.001$; one-way ANOVA.

in vivo, through the induction of an EAU model, and in vitro, where microglia-mediated inflammation was induced. We further constructed a conditional EGR2 knockout mouse strain and found that EGR2 deficiency resulted in an increased intraocular inflammation. Meanwhile, overexpression of EGR2 in vitro alleviated the inflammatory response induced by both LPS and IFN-γ in HMC3 cells. Mechanistically, GDF15 was identified by RNA-seq, and ChIP-PCR showed that EGR2 positively regulated GDF15 expression. Subsequent experiments confirmed that the addition of rbGDF15 ameliorated the progression of EAU, while inhibition of GDF15 reversed the inflammatory phenotype of microglia. These findings collectively indicate that EGR2 actively participates in the inflammatory process and emerges as a potential therapeutic target for uveitis.

The pathogenesis of uveitis remains unclear, but available studies have demonstrated the involvement of various immune cells in its aberrant autoimmune response. The immunopathological function of Th1 and Th17 cells has been demonstrated in several reports, and T cell dysfunction is an important inducer of AU (30–32). Recent studies have emphasized the essential role of microglia in triggering the development of EAU (15, 33). In our study, EAU scRNA-seq data showed that microglia accounted for the majority of retinal immune cells, and immunofluorescence results showed an increased number and morphological changes

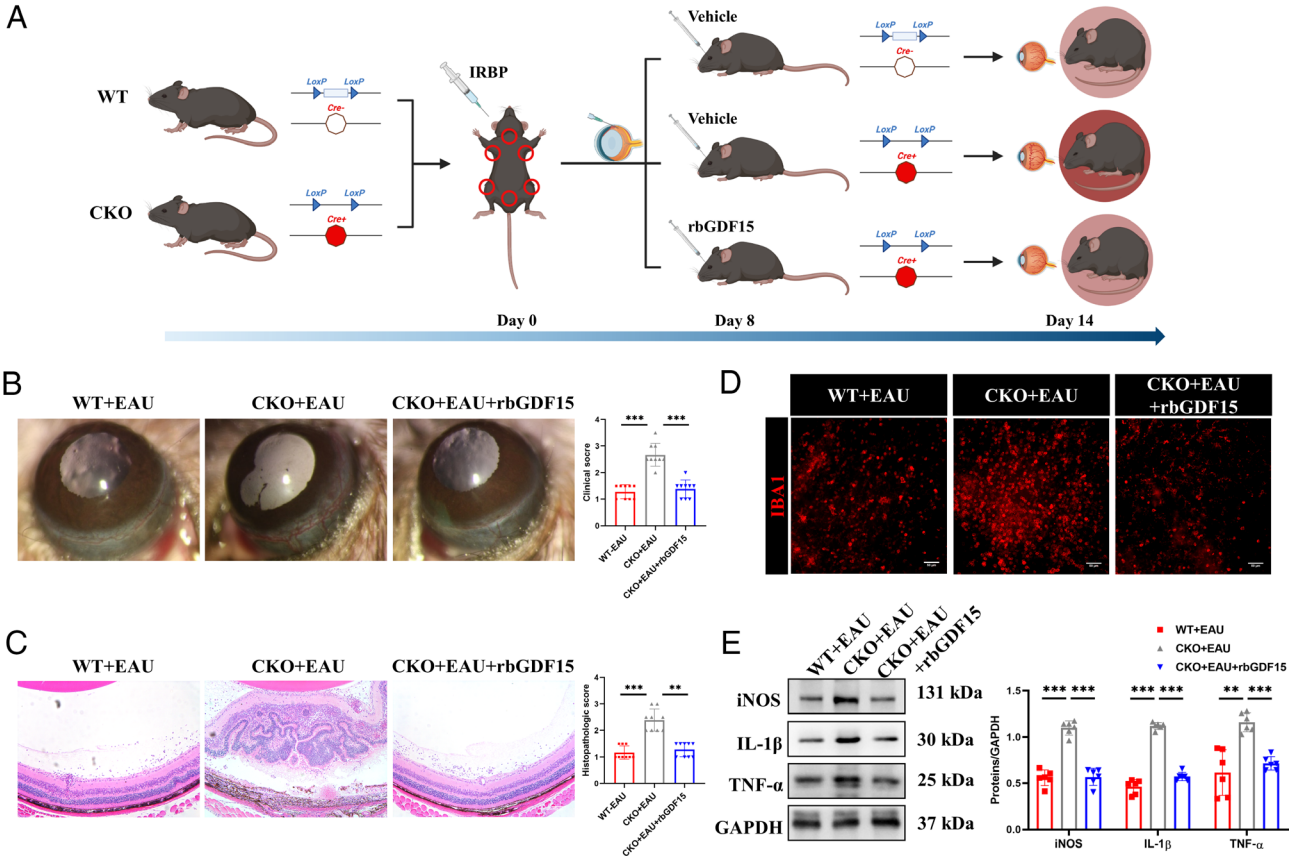


**Fig. 7.** Recombinant GDF15 alleviated EAU progression in vivo. (*A*) Schematic of animal experimental design. (*B* and *C*) Anterior chamber inflammation and retinal histopathological staining of WT+EAU, CKO+EAU, and CKO+EAU+rbGDF15 groups. Clinical scores and pathology scores were also shown (n = 9). (Scale bar, 100 μm.) $^{*}P < 0.05$; $^{**}P < 0.01$; Kruskal–Wallias test. (*D*) Retinal microglia fluorescence staining in the WT+EAU, CKO+EAU, and CKO+EAU+rbGDF15 groups (n = 3). (Scale bar, 50 μm.) (*E*) Protein expression of iNOS, IL-1β, and TNF-α in retina detected using western blotting (n = 6). $^{*}P < 0.05$; $^{**}P < 0.01$; $^{***}P < 0.001$; one-way ANOVA.

of microglia at the peak of inflammation, suggesting the critical role of microglia in the development of EAU, which is consistent with previous reports (15, 16). Furthermore, our studies found decreased expression of EGR2 both in EAU and in LPS & IFN-γ-stimulated microglia cells.

Given the genetic studies on uveitis, particularly in VKH disease, we focused our attention on the role of EGR2 in AU (25–29). VKH disease is a type of autoimmune disease that involves multiple organs and systems in the body and is mainly manifested as diffuse and exudative uveitis in both eyes, accompanied by systemic signs such as alopecia, poliosis, leukodermia, tinnitus, and hearing loss (1). Our previous work involving an iPSC-based retinal pigment epithelium (RPE) cell model of VKH disease demonstrated reduced EGR2 expression in patient-derived RPE, accompanied by impaired RPE cell function (34). Furthermore, targeting EGR2 with a small molecular compound rescued the barrier and phagocytic functions of RPE cells, underscoring the significance of EGR2 in uveitis. Increasing evidence suggests that EGR2 regulates a wide range of immune responses, maintaining autoimmune dynamic homeostasis (35–37). Notably, EGR2 in microglia is considered as a marker of M2 polarisation, exerting neuroprotective, and anti-inflammatory effects (38, 39). However, the underlying mechanism of how EGR2 in microglia contributes to AU development remains unclear. Several microglia-specific mice strains have been developed and have become indispensable tools in investigating microglial function (40). CX3CR1 is a commonly accepted marker for microglia, and its promoter has been widely used to generate genetically modified animals for microglial-specific expression/deletion of targeted genes (41). To address this, we constructed an EGR2 CKO model, revealing that knockout of EGR2 aggravated the EAU immune response, suggesting its protective and anti-inflammatory activities in vivo. Similarly, overexpression of EGR2 inhibited microglial activation in vitro, indicating a negative correlation between EGR2 expression and inflammation. However, we have not observed any systemic, extraocular manifestation such as depigmentation in the EGR2 CKO mice. It is possible the single gene knockout may not adequately recapitulate the general phenotypes including extraocular manifestations.

GDF15, a member of the transforming growth factor beta (TGF-β) family, circulates in plasma as a 25-kDa dimer (42, 43). Normally, GDF15 expression levels are low under physiological conditions but are notably upregulated in tissues and blood in the face of cellular stress signals such as hypoxia, inflammation, and tissue damage (44, 45). Interestingly, the upregulation in pathological conditions appears contradictory to the protective role attributed to GDF15. However, several studies have demonstrated that elevated GDF15 expression serves as a compensatory mechanism for physiological regulation in various diseases (46). For example, GDF15 has been shown to facilitate IL-10 production in regulatory T (Treg) cells, ameliorating the aging-triggered metabolic phenotype and systemic inflammation by enhancing Treg cell-mediated suppression of conventional T cell activation (47, 48). In sepsis, GDF15 inhibits LPS-induced macrophage M1 polarization and promotes M2 polarization, while enhancing their phagocytic and bactericidal functions as a means of attenuating the inflammatory response and promoting pathogen clearance (49). Additionally, GDF15 exerts disease-modifying

functions in SLE by inhibiting lymphocyte proliferation and humoral immunity (50). All these findings suggest that GDF15, as an endocrine hormone, plays an anti-inflammatory role in immune regulation. GDF15 knockout has been reported to significantly increase lung pathology in mice with inhalation-induced acute lung injury (ALI), with increased expression of inflammation-related cytokines and chemokines, and resulted in reduced body weight and shortened survival (51). In addition, GDF15 knockout impaired locomotor recovery in spinal cord injury and dampened the secondary tissue loss by regulating inflammatory cell infiltration, while GDF15 overexpression improved functional outcome (52). Mouse Genome Informatics (MGI) data also presents the symptoms of the central nervous system of GDF15 knockout mice, indicating that GDF15 knockout may exhibit a similar inflammatory phenotype similar to that of EGR2 knockout, which affected the outcome of inflammation-related diseases by participating in the regulation of immune response. Further studies are needed to elucidate the role and the impact of GDF15 knockout on the phenotype of uveitis. However, there was no significant difference in the *GDF15* mRNA expression in PBMC between VKH patients and healthy individuals, which may be due to a cell specificity in the pathogenic effect of GDF15 or the small sample size. We would like to understand the role of GDF15 in uveitis in future studies, which will include but not be limited to patient iPSC-derived RPE and more clinical samples from patients with uveitis. In this study, RNA-seq results indicated significant effects related to growth factor binding and receptor ligand activity in terms of molecular function. GDF15 was identified among the DEGs, and it was confirmed that EGR2 can directly bind to GDF15 and promote its transcription. Our experiments confirmed that knockdown of GDF15 exacerbated inflammation in HMC3 cells, while intravitreal injection of rbGDF15 ameliorated EAU inflammation in EGR2 CKO mice. Therefore, we proposed that GDF15 could play a prominent role as a new biomarker and candidate drug target in the treatment of AU.

Several limitations of this study merit consideration. First, the detailed mechanism of the anti-inflammatory effects exerted by GDF15 in uveitis remains to be further elucidated. Additionally, the small number of primary microglia in retina obtained for experimentation are acknowledged weaknesses. Further studies are supposed to aim at evaluating the efficacy of EGR2 and GDF15 in clinical samples to evaluate their translational value.

In conclusion, this study showed that the conditional knockout of EGR2 exacerbates disease manifestations in EAU mice, whereas EGR2 overexpression mitigates the inflammatory phenotype of microglia. Furthermore, we identified GDF15 as a downstream target of EGR2, suggesting that modulation of GDF15 could counteract the protective effects of EGR2 in the context of inflammatory responses. The current investigation offers avenues for delving into the underlying mechanisms of AU and developing of potent therapeutic targets for autoimmune diseases.

## 3. Methods

**3.1. Animals.** Wild C57BL/6J mice were purchased from the Experimental Animal Center of Chongqing Medical University. $Egr2^{fl/fl}$ mice were purchased from Beijing Weishang Lide Biotechnology Co., Ltd. (Beijing, China). Cx3cr1-Cre transgenic mice were purchased from Saiye Biotechnology Co., Ltd, (Suzhou, China). To generate Egr2 conditional knockout in microglia, we crossed $Cx3cr1^{Cre/Cre}$ mice with $Egr2^{flox/flox}$ mice. Mice with microglia-specific deletion of Egr2 at 6 to 8 wk and their wild-type littermates were used as controls in this experiment. The mice were raised in a specific pathogen-free facility. The experiments were approved by the Ethics Committee of the First Affiliated Hospital of Chongqing Medical University (No. 2019-296). All relevant operators have been trained in animal experiments. All procedures were carried out according to the ARVO Statement for the Use of Animals in Ophthalmic and Vision Research.

**3.2. EAU Induction and Treatment.** Female C57BL/6J mice were subcutaneously immunized with 350 μg of human $IRBP_{651–670}$ (LAQGAYRTAVDLESLASQLT) (Sangon Bioengineering Technology and Services Co., Ltd., Shanghai, China) dissolved in phosphate-buffered saline (PBS), and emulsified with an equal volume of complete Freund's adjuvant (Sigma-Aldrich, St. Louis, MO) containing *Mycobacterium tuberculosis* strain H37Ra (1:1, v/v) (BD Biosciences, NJ). At the same time, the mice received 1 μg of *Bordetella pertussis* toxin in the peritoneum (Sigma-Aldrich, St. Louis, MO). On day 14 after immunization, the clinical symptoms of EAU were examined by a slit lamp. The clinical severity of ocular inflammation was assessed in a masked manner by two independent observers and scored on a 0.5-point scale (in half-point increments) based on five independent criteria and Caspi's criteria (53). During the experiment, we did not observe any unnatural animal deaths.

**3.3. Haematoxylin and Eosin (H&E) Staining.** Mice were killed 14 d after immunization, and the eyeballs were enucleated, fixed, and immersed in PBS with 10% formaldehyde and 5% glacial acetic acid. The dehydrated tissue was embedded in paraffin wax and sectioned to 4 to 6 μM thickness. Sections were stained with H&E, and each eye was scored according to Caspi's criteria (53).

**3.4. Immunofluorescence Staining.** The eyes were removed on day 14 and immediately immersed in 4% paraformaldehyde for 2 h. The cornea, lens, sclera, and vitreous were removed, and the retina was carefully stripped and washed in cold PBS. Second, the retina was placed as a flat mount on the slide with the vitreous facing up and incubated with a PBS solution containing 3% Triton-X for 15 min, followed by blocking with goat serum for 1 h. The retina was incubated with IBA1 (1:1,000, Wako, Japan) at 4 °C overnight. After washing, it was incubated with cy3-conjugated AffiniPure goat anti-rabbit IgG (H + L) (1:1,000, Servicebio, Wuhan, China) for 1 h at room temperature. Photos were taken with a confocal microscope (Zeiss, Germany).

**3.5. Flow Cytometry Analysis.** The mouse retina was removed, soaked in a solution prepared with 0.25% pancreatic enzyme +0.2 μg/mL DNA I enzyme, digested at 37 °C for 30 min, terminated with PBS, and filtrated to obtain a single-cell suspension. The cells were stained with CD11b (1 μL/$10^6$ cells, BioLegend, USA) and EGR2 (1 μL/$10^6$ cells, BioLegend, USA) antibodies. Cells were then analyzed with BD FACSAria (USA), and the acquired data were analyzed with FlowJo X.

**3.6. Cell Lines and Cell Culture.** Human microglia cell line (HMC3) was purchased from the American Type Culture Collection (ATCC) and cultured in EMEM medium (ATCC) with 10% foetal bovine serum (Gibco, USA) and 1% penicillin-streptomycin solution (Gibco, USA). Cells were cultured at 37 °C in a humidified atmosphere containing 5% $CO_2$. HMC3 cell lines were further treated with LPS (1 μg/mL) and IFN-γ (500 ng/mL) for 24 h. The control group received an equivalent volume of sterile deionized water.

**3.7. RT-qPCR.** Total RNA from HMC3 was extracted using TRIzol (Invitrogen, San Diego, CA) and reversed with a RT Master Mix for qPCR kit (MedChemExpress, USA). RT-qPCR was conducted with SYBR Green qPCR Master Mix (MedChemExpress, USA). Gene expression was normalized to the level of β-actin and analyzed by the $2^{-\Delta\Delta Ct}$ method. The primers are shown in *SI Appendix*, Table S1.

**3.8. Western Blotting.** We performed western blotting using standard methods. Protein from HMC3 was extracted using the nuclear and cytoplasmic protein extraction kit (Beyotime, Shanghai, China), and the protein concentration was measured using a bicinchoninic acid assay kit (Beyotime, Shanghai, China). An equal amount of 20 μg protein was separated by 6 to 15% SDS-polyacrylamide gel electrophoresis. The separated proteins were electrotransferred onto polyvinylidene difluoride membranes (Millipore, MA). The membranes were blocked with 5% skim milk for 2 h and incubated with primary antibodies for 16 h at 4 °C. Primary antibodies including iNOS (1:1,000, Proteintech, 18985-1-AP), IL-1β (1:1,000, Abcam, ab283818), TNF-α (1:1,000, Abcam, ab183218), EGR2 (1:1,000, Abcam, ab183218), GDF15 (1:1,000, Proteintech, 27455-1-AP), and GAPDH (1:4,000, Proteintech, 60004–1-Ig) were used as internal references. The membrane was washed with Tris-buffered saline with 0.1% Tween-20 and

incubated with HRP-affinipure goat anti-rabbit IgG (1:6,000, Proteintech, SA00001-2) or HRP-AffiniPure goat anti-mouse IgG secondary antibodies (1:6,000, Proteintech, SA00001-1) for 1 h at room temperature. The membrane was visualized using an ECL kit (Thermo, USA), and band densitometry was quantified using Image J.

**3.9. Wound Healing Assay.** HMC3 cells were inoculated in a six-well plate, and a scratch was made vertically on the plate from top to bottom. After washing with PBS, the scratch was observed and photographed under an inverted microscope. Fresh medium with or without LPS and IFN-γ was added and continued to be cultured for 24 h. The scratches were observed and photographed again the next day after washing. Image J software was used to analyze the scratch area. Migration ratio = (0 h to 24 h area)/0 h area.

**3.10. Transwell Assay.** A transwell chamber (Corning, USA) was employed in the migration assay. A total of 1.5 to 2 × $10^4$ HMC3 cells were plated in the upper chamber. The culture medium was changed to EMEM with 10% FBS in the lower chamber and EMEM with 2% FBS in the upper chamber and cultured for 24 h with or without LPS and IFN-γ stimulation. Then, 4% paraformaldehyde was used to submerge the upper chamber and fix it for 20 min. After washing, the crystal violet dyeing solution was added to the upper chamber for staining. Finally, we removed the upper chamber, placed it on a slide, and used an inverted microscope to observe and take photos. Image J was used to count the stained cells to compare the migration abilities of different treated cells.

**3.11. 5-Ethynyl-2-Deoxyuridine (EdU) Assay.** HMC3 cells were counted and cultured with 2 × $10^4$ cells per well in a 24-well plate on which a cell slide had been placed in advance. A total of 2 × EdU working solution (Beyotime, China) equal in volume to medium was added and incubated for 2 h. The cells were permeabilized and fixed. Then, cells were incubated with the reaction solution at room temperature and away from light for 30 min. After staining the nuclei with Hoechst33342, stained cells were photographed by fluorescence microscopy. Stained cells were counted using Image J to compare cell proliferation.

**3.12. Cell Transfection.** EGR2 overexpression lentivirus was designed and provided by Hanheng Biotech Co., Ltd. (Shanghai, China), and GDF15 knockdown lentivirus was designed and provided by Sangon Bioengineering Technology and Services Co., Ltd. (Shanghai, China). The virus was transfected into HMC3 cells, and an equal amount of complete EMEM medium was added 4 to 6 h later, with a normal medium change the next day. After 72 h of transfection, cells with high transfection efficiency and good status were screened under a fluorescence microscope. A complete EMEM medium containing 2 μg/mL puromycin was added to screen for stable cell lines.

**3.13. RNA-seq.** Cell RNA was first extracted with TRIzol. Sample quality inspection, library construction, and transcriptome analysis were strictly controlled and completed by Novogene Biotechnology Co., Ltd. (Beijing, China). Different-expressed genes (DEGs) were identified according to padj $< 0.05$ and $|\log_2(\text{fold change})(\log_2 FC)| > 1$.

**3.14. ChIP Assay.** HMC3 cells were washed and scraped off at a low temperature and centrifuged at 4 °C for 5 min. The cells were collected, frozen in liquid nitrogen for 5 min, and stored at −80 °C. Sample cross-linking, nuclear separation, WB verification, nucleic acid quality inspection, nucleic acid enrichment, and ChIP-PCR library construction were strictly controlled and completed by Seqhealth Technology Co., Ltd. (Wuhan, China). The primers used are shown in *SI Appendix*, Table S2.

**3.15. Intravitreal Injection.** Recombinant GDF15 protein (R&D Systems, USA, Catalog #8944-GD-025) was injected into the mouse vitreous with a Hamilton syringe at 10 μM with a total volume of 1 μL on day 8 after EAU modeling, and the control group was injected with the same volume of vehicle solution by the same method.

**3.16. Study Participants.** This study included 5 patients with VKH disease and 5 healthy individuals. All patients were diagnosed VKH disease according to the diagnostic criteria revised for VKH disease by the International Committee on Nomenclature (54). The study was approved by the Ethics Committee of The First Affiliated Hospital of Chongqing Medical University (NO.2018–048). Signed informed consent was obtained from all participants at the beginning of the study. All procedures were performed in accordance with the Declaration of Helsinki. Peripheral blood mononuclear cells (PBMCs) were purified from heparinized blood using Ficoll-Hypaque density gradient centrifugation for further experiments.

**3.17. Statistical Analysis.** All data were statistically analyzed using SPSS Statistics 20.0 (IBM, USA). Unpaired Student's *t* test was used between two groups of samples, and one-way ANOVA was used for analysis of multiple groups. For clinical and pathological scores, the Mann–Whitney *U* test was used in two groups and the Kruskal–Wallis test in multiple groups. The differences were considered to be statistically significant at $P < 0.05$.

**Data, Materials, and Software Availability.** All study data are included in the article and/or supporting information. RNA-seq data have been submitted to Sequence Read Archive (SRA) under accession number PRJNA1156555 (55).

**ACKNOWLEDGMENTS.** This work was supported by National Natural Science Foundation Project of China (82070951, 82271078, 82371045); Beijing Municipal Public Welfare Development and Reform Pilot Project for Medical Research Institutes (PWD&RPP-MRI, JYY2023-6), the Chongqing Natural Science Foundation (CSTB2022NSCQ-MSX0144), and Program for Youth Innovation in Future Medicine, Chongqing Medical University (w0047).

Author affiliations: [a]The First Affiliated Hospital of Chongqing Medical University, Chongqing Key Laboratory of Ophthalmology, Chongqing Eye Institute, Chongqing Branch (Municipality Division) of National Clinical Research Center for Ocular Diseases, Chongqing 400016, China; [b]Department of Laboratory Medicine, Beijing Tongren Hospital, Capital Medical University, Beijing 100005, China; and [c]Department of Beijing Institute of Ophthalmology, Beijing Tongren Eye Center, Beijing Tongren Hospital, Capital Medical University, Beijing 100730, China

Author contributions: W.L., S. He, J.T., K.H., P.Y., and S. Hou designed research; W.L., S. He, J.T., C.Z., X.W., Z.Z., J.L., J.H., X.L., and Q.Z. performed research; W.L. and S. He contributed new reagents/analytic tools; W.L., S. He, J.T., N.L., and X.W. analyzed data; and W.L. and J.T. wrote the paper.

1. S. Hou, N. Li, X. Liao, A. Kijlstra, P. Yang, Uveitis genetics. *Exp. Eye Res.* **190**, 107853 (2020).
2. B. M. Burkholder, D. A. Jabs, Uveitis for the non-ophthalmologist. *BMJ* **372**, m4979 (2021), 10.1136/bmj.m4979.
3. Z. Zhong, G. Su, A. Kijlstra, P. Yang, Activation of the interleukin-23/interleukin-17 signalling pathway in autoinflammatory and autoimmune uveitis. *Prog. Retin. Eye Res.* **80**, 100866 (2021).
4. J. Hu *et al.*, Gut microbiota-mediated secondary bile acids regulate dendritic cells to attenuate autoimmune uveitis through TGR5 signaling. *Cell Rep.* **36**, 109726 (2021).
5. G. Wang *et al.*, Icariin alleviates uveitis by targeting peroxiredoxin 3 to modulate retinal microglia M1/M2 phenotypic polarization. *Redox Biol.* **52**, 102297 (2022).
6. J. Tan *et al.*, Small molecules targeting RORγt inhibit autoimmune disease by suppressing Th17 cell differentiation. *Cell Death Dis.* **11**, 697 (2020).
7. X. Liu *et al.*, A de novo missense mutation in MPP2 confers an increased risk of Vogt-Koyanagi-Harada disease as shown by trio-based whole-exome sequencing. *Cell Mol. Immunol.* **20**, 1379–1392 (2023).
8. N. Shu *et al.*, Apigenin alleviates autoimmune uveitis by inhibiting microglia M1 pro-inflammatory polarization. *Invest. Ophthalmol. Vis. Sci.* **64**, 21 (2023).
9. J. Meng *et al.*, NLRP3 attenuates intraocular inflammation by inhibiting AIM2-mediated pyroptosis through the phosphorylated salt-inducible kinase 1/sterol regulatory element binding transcription factor 1 pathway. *Arthritis Rheumatol.* **75**, 842–855 (2023).
10. J. Meng *et al.*, METTL3 inhibits inflammation of retinal pigment epithelium cells by regulating NR2F1 in an m6A-dependent manner. *Front. Immunol.* **13**, 905211 (2022).
11. H. Li *et al.*, Aging weakens Th17 cell pathogenicity and ameliorates experimental autoimmune uveitis in mice. *Protein Cell* **13**, 422–445 (2022).
12. Y. Liu *et al.*, Galectin-3 regulates microglial activation and promotes inflammation through TLR4/MyD88/NF-kB in experimental autoimmune uveitis. *Clin. Immunol.* **236**, 108939 (2022).
13. S. He *et al.*, FTO-mediated m6A modification alleviates autoimmune uveitis by regulating microglia phenotypes via the GPC4/TLR4/NF-κB signaling axis. *Genes Dis.* **10**, 2179–2193 (2023).
14. H. Zhou *et al.*, Low expression of YTH domain-containing 1 promotes microglial M1 polarization by reducing the stability of sirtuin 1 mRNA. *Front. Cell. Neurosci.* **15**, 774305 (2021).
15. Y. Okunuki *et al.*, Retinal microglia initiate neuroinflammation in ocular autoimmunity. *Proc. Natl. Acad. Sci. U.S.A.* **116**, 9989–9998 (2019).
16. W. Fan *et al.*, Retinal microglia: Functions and diseases. *Immunology* **166**, 268–286 (2022).
17. E. Murenu, M.-J. Gerhardt, M. Biel, S. Michalakis, More than meets the eye: The role of microglia in healthy and diseased retina. *Front. Immunol.* **13**, 1006897 (2022).
18. C. Zhao *et al.*, LGALS3BP in microglia promotes retinal angiogenesis through PI3K/AKT pathway during hypoxia. *Invest. Ophthalmol. Vis. Sci.* **63**, 25 (2022).

19. L. J. Joseph *et al.*, Molecular cloning, sequencing, and mapping of EGR2, a human early growth response gene encoding a protein with "zinc-binding finger" structure. *Proc. Natl. Acad. Sci. U.S.A.* **85**, 7164–7168 (1988).
20. N. Le *et al.*, Analysis of congenital hypomyelinating Egr2 $^{Lo/Lo}$ nerves identifies Sox2 as an inhibitor of Schwann cell differentiation and myelination. *Proc. Natl. Acad. Sci. U.S.A.* **102**, 2596–2601 (2005).
21. K. Morita *et al.*, Egr2 and Egr3 in regulatory T cells cooperatively control systemic autoimmunity through Ltbp3-mediated TGF-β3 production. *Proc. Natl. Acad. Sci. U.S.A.* **113**, E8131–E8140 (2016).
22. Z. Czimmerer *et al.*, The epigenetic state of IL-4–polarized macrophages enables inflammatory cistromic expansion and extended synergistic response to TLR ligands. *Immunity* **55**, 2006–2026.e6 (2022).
23. T. Veremeyko, A. W. Y. Yung, D. C. Anthony, T. Strekalova, E. D. Ponomarev, Early growth response gene-2 is essential for M1 and M2 macrophage activation and plasticity by modulation of the transcription factor CEBPβ. *Front. Immunol.* **9**, 2515 (2018).
24. G. Cai *et al.*, Network analysis of miRNA and mRNA changes in the prelimbic cortex of rats with chronic neuropathic pain: Pointing to inflammation. *Front. Genet.* **11**, 612 (2020).
25. S. Hou *et al.*, Genome-wide association analysis of Vogt-Koyanagi-Harada syndrome identifies two new susceptibility loci at 1p31.2 and 10q21.3. *Nat. Genet.* **46**, 1007–1011 (2014).
26. T. Sakono *et al.*, Variants in IL23R-C1orf141 and ADO-ZNF365-EGR2 are associated with susceptibility to Vogt-Koyanagi-Harada disease in Japanese population. *PLoS One* **15**, e0233464 (2020).
27. S. Cao *et al.*, Investigation of the association of Vogt–Koyanagi–Harada syndrome with IL23R-C1orf141 in Han Chinese Singaporean and ADO-ZNF365-EGR2 in Thai. *Br. J. Ophthalmol.* **100**, 436–442 (2016).
28. M. Takeuchi *et al.*, Dense genotyping of immune-related loci implicates host responses to microbial exposure in Behçet's disease susceptibility. *Nat. Genet.* **49**, 438–443 (2017).
29. P. Wu *et al.*, Association of *LACC1, CEBPB - PTPN1, RIPK2* and *ADO-EGR2* with ocular Behcet's disease in a Chinese Han population. *Br. J. Ophthalmol.* **102**, 1308–1314 (2018).
30. M. Zhang, X. Zhang, T cells in ocular autoimmune uveitis: Pathways and therapeutic approaches. *Int. Immunopharmacol.* **114**, 109565 (2023).
31. W. Fan *et al.*, Global lactylome reveals lactylation-dependent mechanisms underlying $T_H$ 17 differentiation in experimental autoimmune uveitis. *Sci. Adv.* **9**, eadh4655 (2023).
32. H. Li *et al.*, Aging weakens Th17 cell pathogenicity and ameliorates experimental autoimmune uveitis in mice. *Protein Cell* **13**, 422–445 (2022).
33. M. Karlstetter *et al.*, Retinal microglia: Just bystander or target for therapy? *Prog. Retin. Eye Res.* **45**, 30–57 (2015).
34. W. Li *et al.*, iPSC-based model of Vogt-Koyanagi-Harada disease for phenotype recapitulation and drug screening. *Clin. Immunol.* **246**, 109205 (2023).
35. K. Morita *et al.*, Emerging roles of Egr2 and Egr3 in the control of systemic autoimmunity. *Rheumatology* **55**, ii76–ii81 (2016).
36. T. Miao *et al.*, Egr2 and 3 control adaptive immune responses by temporally uncoupling expansion from T cell differentiation. *J. Exp. Med.* **214**, 1787–1808 (2017).
37. M. V. Wagle *et al.*, Antigen-driven EGR2 expression is required for exhausted CD8+ T cell stability and maintenance. *Nat. Commun.* **12**, 2782 (2021).
38. N. Serikuly *et al.*, Effects of acute and chronic arecoline in adult zebrafish: Anxiolytic-like activity, elevated brain monoamines and the potential role of microglia. *Prog. Neuropsychopharmacol. Biol. Psychiatry* **104**, 109977 (2021).
39. Y. Fan *et al.*, MiR-377 regulates inflammation and angiogenesis in rats after cerebral ischemic injury. *J. Cell. Biochem.* **119**, 327–337 (2018).
40. C. N. Parkhurst *et al.*, Microglia promote learning-dependent synapse formation through brain-derived neurotrophic factor. *Cell* **155**, 1596–1609 (2013).
41. S. Hickman, S. Izzy, P. Sen, L. Morsett, J. El Khoury, Microglia in neurodegeneration. *Nat. Neurosci.* **21**, 1359–1369 (2018).
42. S. E. Mullican *et al.*, GFRAL is the receptor for GDF15 and the ligand promotes weight loss in mice and nonhuman primates. *Nat. Med.* **23**, 1150–1157 (2017).
43. L. Yang *et al.*, GFRAL is the receptor for GDF15 and is required for the anti-obesity effects of the ligand. *Nat. Med.* **23**, 1158–1166 (2017).
44. Z. Wang *et al.*, GDF15 induces immunosuppression via CD48 on regulatory T cells in hepatocellular carcinoma. *J. Immunother. Cancer* **9**, e002787 (2021).
45. D. Wang *et al.*, GDF15: Emerging biology and therapeutic applications for obesity and cardiometabolic disease. *Nat. Rev. Endocrinol.* **17**, 592–607 (2021).
46. A. Assadi, A. Zahabi, R. A. Hart, GDF15, an update of the physiological and pathological roles it plays: A review. *Pflugers Arch. Eur. J. Physiol.* **472**, 1535–1546 (2020).
47. J. S. Moon *et al.*, Growth differentiation factor 15 protects against the aging-mediated systemic inflammatory response in humans and mice. *Aging Cell* **19**, e13195 (2020).
48. M. Conte *et al.*, GDF15, an emerging key player in human aging. *Ageing Res. Rev.* **75**, 101569 (2022).
49. H. Li *et al.*, The clinical value of GDF15 and its prospective mechanism in sepsis. *Front. Immunol.* **12**, 710977 (2021).
50. G. Lorenz *et al.*, GDF15 suppresses lymphoproliferation and humoral autoimmunity in a murine model of systemic lupus erythematosus. *J. Innate Immun.* **14**, 673–689 (2022).
51. M. Deng *et al.*, Gdf15 deletion exacerbates acute lung injuries induced by intratracheal inoculation of aerosolized ricin in mice. *Toxicology* **469**, 153135 (2022).
52. M. Hassanpour Golakani *et al.*, MIC-1/GDF15 overexpression is associated with increased functional recovery in traumatic spinal cord injury. *J. Neurotrauma* **36**, 3410–3421 (2019).
53. R. K. Agarwal, P. B. Silver, R. R. Caspi, "Rodent Models of Experimental Autoimmune Uveitis" in *Autoimmunity*, A. Perl, Ed. (*Methods in Molecular Biology*, Humana Press, 2012), pp. 443–469.
54. R. W. Read *et al.*, Revised diagnostic criteria for Vogt-Koyanagi-Harada disease: Report of an international committee on nomenclature. *Am. J. Ophthalmol.* **131**, 647–652 (2001).
55. W. Li *et al.*, Transcription factor EGR2 alleviates autoimmune uveitis via activation of GDF15 to modulate the retinal microglial phenotype. NCBI SRA database. https://www.ncbi.nlm.nih.gov/sra/PRJNA1156555. Deposited 4 Sep 2024.